[6]Ghielmi, L. G., Marazzi, R., and Baron, A., "A Tool for Automatic Design of Airfoils in Different Operating Conditions," AGARD CP-463, Loen, Norway, 1989.

Dihedral for Spiral Stability

Amnon Katz*
University of Alabama,
Tuscaloosa, Alabama 35487-0280

Nomenclature

a = airframe acceleration
b = wingspan
C_{Lw} = lift coefficient of the wing
c = wing chord
c_l = lift coefficient of a wing section, two dimensional
g = magnitude of the acceleration of gravity
l_f = moment arm of the fin (vertical tail)
M = moment
S = wing area
V = airframe velocity, relative to the air mass
x = body coordinate positive forward
y = body coordinate positive to the right
z = body coordinate positive down
α_f = angle of attack of the fin (vertical tail)
α_w = wing angle of attack
α_{w0} = zero lift angle of attack of the wing
α_{w1} = modified angle of attack of the wing
β = angle of sideslip
Γ = wing dihedral angle
Γ_0 = wing dihedral angle for neutral spiral stability
η = dimensionless spanwise variable, $2y/b$
ϕ = bank angle
ω = angular velocity

I. Introduction

THIS Note sets forth a rule of thumb to determine the wing dihedral angle that assures lateral stability in a low-speed airframe. The amount of dihedral Γ_0 that corresponds to neutral stability against the spiral mode is related to the wing angle of attack, measured from zero lift, and to the ratio of wingspan to fin moment arm:

$$\Gamma_0 = \kappa(b/l_f)(\alpha_w - \alpha_{w0}) \tag{1}$$

Section II offers an approximate, "back of the envelope" derivation of (1), assuming a rectangular spanwise lift distribution. Section III compares the predicted Γ_0 to data obtained from a full six degrees-of-freedom dynamic computer simulation. Section IV refines the analysis to address a general lift distribution. The value of κ in (1) depends on the shape of the distribution. Sample values are

$$\kappa = \begin{cases} \frac{2}{3} \approx 0.67 \text{ (rectangular)} \\ 3\pi/16 \approx 0.59 \text{ (elliptic)} \\ \frac{1}{2} = 0.50 \text{ (triangular)} \end{cases} \tag{2}$$

Received Aug. 10, 1994; revision received Nov. 28, 1994; accepted for publication Dec. 15, 1994.

*Professor, Department of Aerospace Engineering, P.O. Box 870280. Member AIAA.

II. Rudimentary Analysis

A forward, right, down body system of coordinates is used throughout. Components of vectors are in the body system and are denoted by subscripts x, y, z.

When an airplane is banked at an angle ϕ, gravity produces a lateral acceleration

$$a_y = g \sin\phi \tag{3}$$

This causes the trajectory to curve. The fin (vertical tail), acting as a weathervane, forces the airplane to turn and remain approximately aligned with the curved trajectory. The rate of turn is

$$\omega_z = a_y/V = (g/V)\sin\phi \tag{4}$$

The yaw rate creates an asymmetrical flow over the airframe. The wing on the outside of the turn travels faster than the wing on the inside, creating more lift, and therefore, a rolling moment into the turn, hence, spiral instability.

The local velocity along the wing is $V + \omega_z y$. The first-order rolling moment that results is

$$M_{1x} = \rho V \omega_z \int_{-(b/2)}^{b/2} c_l c y^2 \, dy \tag{5}$$

Assume a rectangular lift distribution

$$c_l c = C_{Lw} S/b \tag{6}$$

where C_{Lw} is the lift coefficient of the wing. When (6) is substituted in (5), one finds

$$M_{1x} = \tfrac{1}{12} C_{Lw} \rho S V \omega_z b^2 \tag{7}$$

Converted to a moment coefficient (normalized to the volume bS) this becomes

$$C_{M1x} = C_{Lw}(b\omega_z/6V) = C_{Lw}(bg/6V^2)\sin\phi \tag{8}$$

This rolling moment tends to increase the bank. To insure spiral stability, it must be canceled and reversed by some other rolling moment.

The asymmetrical flow also creates yawing tendencies. One way that this arises is through increased drag on the outside wing, which tends to yaw the nose of the airplane to the outside of the turn. This effect may be calculated similarly to Eq. (5), but with lift replaced by drag. The effect is much smaller because wing drag is much smaller than wing lift. We will neglect this contribution.

A more significant effect is produced by the fin. The yawing creates a side flow at the fin in the amount of $\omega_z l_f$. Given this lateral flow and any sideslip angle β that may exist, the angle of attack of the fin becomes

$$\alpha_f = \beta - (l_f \omega_z / V) \tag{9}$$

The weathervane effect forces this angle of attack to zero, creating a sideslip angle

$$\beta = l_f \omega_z / V = (l_f g/V^2)\sin\phi \tag{10}$$

The banked and turning airplane, left to its own devices, points towards the outside of the turn. This is a well-known secondary effect. Pilots performing a steady turn compensate by applying rudder into the turn. They also neutralize the moment (5) by applying aileron against the turn.

The passive, controls fixed, airframe actually maintains a sideslip angle while it turns. This is where the effect of dihedral comes in. A dihedral angle Γ combined with a sideslip angle

β changes the effective value of the angle of attack of the wing from α_w to α_{w1}. This is a well-known, purely geometric effect,[1] which, if linearized in all angles, amounts to

$$\alpha_{w1} = \alpha_w \pm \Gamma\beta \tag{11}$$

The angle of attack of the upwind wing increases and that of the downwind wing is reduced. The result is a rolling moment in the amount

$$M_{2x} = -\tfrac{1}{8}C_{Lw\alpha}\Gamma\beta\rho SbV^2 \tag{12}$$

Equation (12) again assumes a rectangular lift distribution.

The moment M_{2x} acts against the turn. Reduced to a coefficient, with β substituted from (10), it becomes

$$C_{M2x} = -\tfrac{1}{4}C_{Lw\alpha}\Gamma(l_f g/V^2)\sin\phi \tag{13}$$

Adding (8) and (13), the rolling moment coefficient becomes

$$C_{Mx} = C_{M1x} + C_{M2x} = C_{Lw}\frac{bg}{6V^2}\left(1 - \frac{3}{2}\frac{C_{Lw\alpha}}{C_{Lw}}\frac{l_f}{b}\Gamma\right)\sin\phi \tag{14}$$

In the last expression we substitute

$$\frac{C_{Lw\alpha}}{C_{Lw}} = \frac{1}{\alpha_w - \alpha_{w0}} \tag{15}$$

to get

$$C_{Mx} = C_{Lw}\frac{bg}{6V^2}\left(1 - \frac{3}{2}\frac{\Gamma}{\alpha_w - \alpha_{w0}}\frac{l_f}{b}\right)\sin\phi \tag{16}$$

The condition for spiral stability is that the coefficient of $\sin\phi$ in (16) be negative. This translates into Γ greater than Γ_0 of Eq. (1), with $\kappa = \frac{2}{3}$.

III. Computer Simulation

One now proceeds to test the rule of thumb (1) against a full, nonlinear, six degree-of-freedom computer simulation.

The airframe model, shown in Fig. 1, is inspired by the Cessna 150, with which it roughly agrees in configuration and weight. The model consists of 19 point masses and 12 aerodynamic panels. The panels are numbered by an index i and the masses by an index k. The c.p. of each panel is indicated by an open circle. Each mass is shown as a shaded sphere. Values of mass and area are indicated on the figure in pounds and square feet, respectively. In the case of the wing panels the mass coincides with the c.p. A typical wing panel weighs 50 lb; the inboard panels (that hold the fuel tanks) are 117.5 lb. No mass was associated with tail panels. The typical fuselage mass is 37.5 lb. Larger masses represent the engine, crew, and baggage. For simplicity, one set of aerodynamic tables is specified for all panels. These tables represent a cambered airfoil, appropriate for the wing. We use this same airfoil, set at a lower incidence, for the horizontal tail. For the vertical tail, we overcome the asymmetry of the panels by superposing two of them, facing opposite ways.

No representation is provided for the aerodynamic effects of the fuselage, landing gear, struts, etc. The double-panel arrangement doubles the effective area of the fin and makes up for missing side area of the fuselage. The big mass in the nose is the engine; however, we do not represent its thrust, but rather study the airframe dynamics, power off.

The program that integrates the dynamic equations and computes the motion of the airframe, AIRPLANE (Ref. 2), is written in C++. The code "includes" the user-defined types

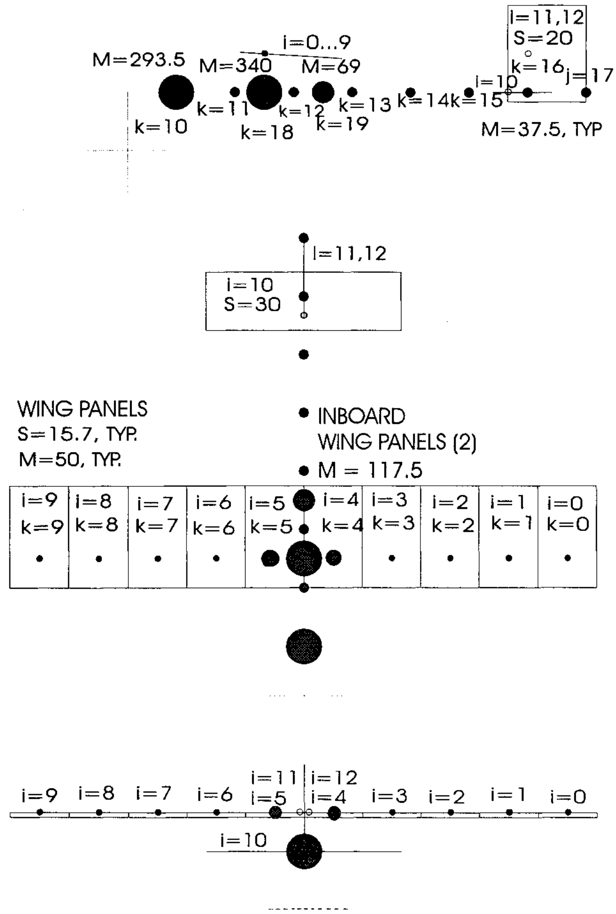

Fig. 1 Airframe model.

for three dimensions.[3,4] The types in question are vector, matrix, and Q (for quaternion). This allows vectors, 3×3 matrices, and quaternions to be represented as single computer variables. In this way the code can be close to the equations, which makes it more compact, more readable, and less prone to error.

The general properties of the airframe are

W = gross weight, 1600 lb
S = wing area, 157 ft^2
b = wingspan, 33.3 ft
S_t = horizontal tail area, 30 ft^2
l_t = horizontal tail moment arm, 11.97 ft
S_f = vertical tail area (each panel), 20 ft^2
l_f = vertical tail moment arm, 13.07 ft
α_{wi} = wing incidence, 3.5 deg
α_{ti} = horizontal tail incidence, 0 deg
α_{w0} = wing zero lift angle of attack, -2.9 deg

The airframe trims out at an angle of attack $\alpha = -1.9$ deg (about 4.5-deg above the wing zero lift) and at a calibrated airspeed of 83 kn.

Figure 2 shows histories of the three components of body system angular velocity $\boldsymbol{\omega}$ computed by AIRPLANE for the zero dihedral airframe. The initial conditions of the simulated flight deliberately included 1 deg of sideslip. The curve of ω_y (pitch) reflects the stable longitudinal short period and phugoid. The lateral components of $\boldsymbol{\omega}$ also undergo a fast and highly damped short period oscillations. When these have decayed, a divergence occurs. ω_x and ω_z slowly grow, showing that the airframe enters a spiral to the right. This is as expected. The Cessna 150 that inspired the model is not stable in the spiral mode, and this is typical of manned aircraft.

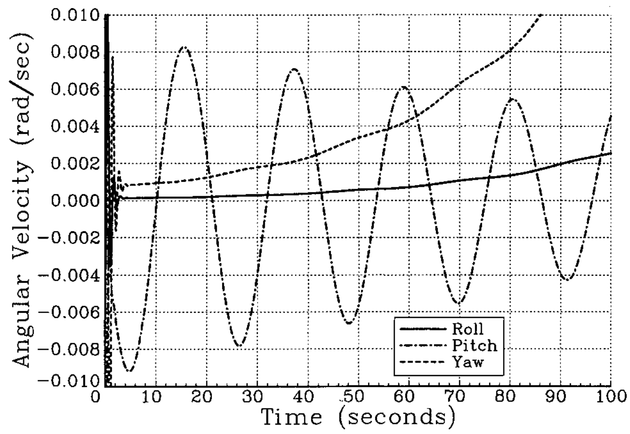

Fig. 2 History of angular velocity (Γ = 0).

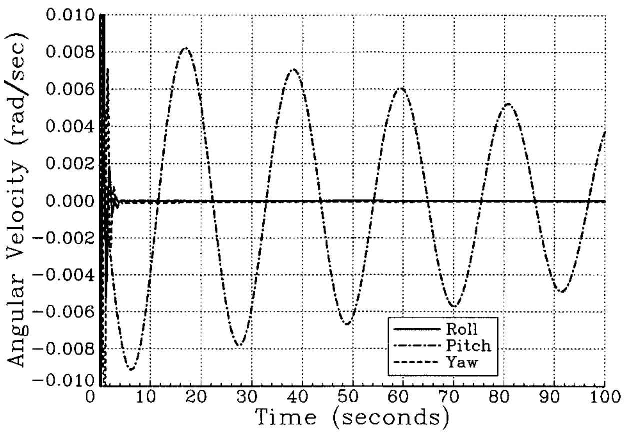

Fig. 3 History of angular velocity (Γ = 8 deg).

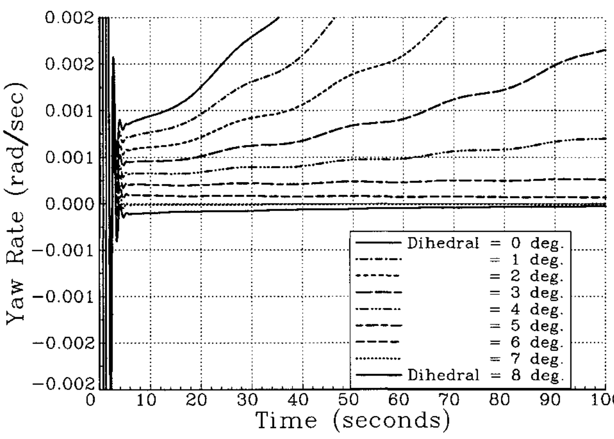

Fig. 4 Effect of dihedral on spiral stability.

Figure 3 shows the time histories of angular rates for an airframe modified only in that the wing dihedral is 8 deg. The initial conditions are the same. One can see that no spiral develops. Figure 4 shows, on an enlarged scale, a sequence of histories of the yaw rate for dihedral varying from zero to 8 deg, in 1-deg increments. Neutral spiral stability is crossed between 6–8 deg of dihedral. The value of Γ_0 predicted by (1) is

$$\Gamma_0 = \frac{2 \times 30 \text{ ft}}{3 \times 13.07 \text{ ft}} [-1.9 \text{ deg} + 3.5 \text{ deg} - (-2.9 \text{ deg})] \approx 6.9 \text{ deg} \tag{17}$$

The results of the computer simulation are subject to the simplifying assumptions embodied in the model. In particular, a rectangular lift distribution is assumed, and steady-state aerodynamic data is used in a dynamic situation. The simulation does compute the six degree-of-freedom dynamics rigorously and allows all rigid airframe modes to interact naturally. It shows that the assumptions of Sec. II, weathervane effects, etc., are substantially correct. The accuracy of the computer simulation is addressed in Appendix A, where it is shown that the values plotted, even at the end of the 100-s interval, are accurate within 2.5%.

IV. Limitations and Extensions

The derivation of Sec. II assumed a rectangular spanwise distribution of lift (6). Now replace (6) by a general symmetric distribution

$$c_l c = (C_{Lw} S/b) f(2y/b) \tag{18}$$

where f is defined on the domain $[-1,1]$, and satisfies

$$f(-\eta) = f(\eta) \tag{19}$$

$$\int_0^1 f(\eta)\, d\eta = 1 \tag{20}$$

This has the effect of replacing M_{1x} of Eq. (7) by

$$M_{1x} = \frac{1}{4} C_{Lw} \rho S V \omega_z b^2 \int_0^1 f(\eta) \eta^2\, d\eta \tag{21}$$

M_{2x} of (12) changes into

$$M_{2x} = -\frac{1}{4} C_{Lw\alpha} \Gamma \beta \rho S b V^2 \int_0^1 f(\eta) \eta\, d\eta \tag{22}$$

When both moments are transformed into coefficients and added together, (14) is replaced by

$$C_{Mx} = C_{M1x} + C_{M2x} = C_{Lw} \frac{bg}{2V^2} \int_0^1 f(\eta)\eta^2\, d\eta \times \left(1 - \frac{1}{\kappa} \frac{C_{Lw\alpha}}{C_{Lw}} \frac{l_f}{b} \Gamma\right) \sin\phi \tag{23}$$

where

$$\kappa = \int_0^1 f(\eta)\eta^2\, d\eta \Bigg/ \int_0^1 f(\eta)\eta\, d\eta \tag{24}$$

The requirement for spiral stability is that the coefficient of $\sin\phi$ in (23) be negative, which leads to (1).

The value of κ, determined by (24), must lie between 0–1. Lift concentration at the centerline leads to low κ; spreading of lift towards the wingtips tends to increase κ. A practical range may lie between the square distribution (Sec. II, $\kappa = \frac{2}{3}$) and the triangular distribution ($\kappa = \frac{1}{2}$).

In the case of the elliptic lift distribution

$$f(\eta) = (4/\pi)\sqrt{1 - \eta^2} \tag{25}$$

The integral in the denominator of (24) may be evaluated by elementary methods and comes to $4/3\pi$. It is shown in Appendix A, by use of the Cauchy integral theorem, that the definite integral in the numerator is $\frac{1}{4}$. Together they yield $\kappa = 3\pi/16 \approx 0.59$.

Equation (1) accounts for the effect of the wing dihedral only. As is well known, other factors such as the placement of the wing, high or low, contribute to rolling moment due

Table A1 Precision at t = 100s

Δt, s	ω_x, rad/s	ω_y, rad/s	ω_z, rad/s
0.01	0.00254935	0.00456295	0.01518767
0.001	426	46752	1564
0.0001	75	5811	840
Error @ Δt = 0.01s	0.00000460	0.00010484	0.00006927
Percentage	0.18%	2.35%	0.45%

to sideslip. An accurate determination of stability and dynamic response requires a more rigorous analysis, and ultimately a detailed simulation or live test. Equation (1) is merely a quick "ballpark" estimate.

Appendix A: Computational Error

The computer program AIRPLANE integrates the six degree-of-freedom rigid airframe equations by an advanced/retarded Euler integration scheme. All computations are carried out double precision (51 bit mantissa—15 digit accuracy). A time step of 0.01 s is used. The solution is constructed for a period of 100s (10,000 steps). With these parameters, the dominant source of error is the use of finite steps. The error builds up with time. It can be reduced by decreasing the integration step Δt.

Table A1 demonstrates that this is indeed so. The values of the three components of $\boldsymbol{\omega}$, computed for t = 100 s (the worst case), are presented. The values obtained with Δt = 0.01 s are compared to ones obtained with Δt = 0.001 s and Δt = 0.0001 s. It is seen that the values converge as Δt is reduced. (Only the digits that change are shown in subsequent lines.)

Accepting $\boldsymbol{\omega}$ at t = 100s computed with Δt = 0.0001 s as ground truth, the errors in the values obtained with Δt = 0.01 s can be found (Table A1). The error in ω_y amounts to 2.35%. The error in the other components is a fraction of a percent.

Appendix B: Evaluation of Definite Integral

The definite integral

$$I = \int_0^1 \sqrt{1 - \eta^2}\eta^2 \, d\eta \tag{B1}$$

is evaluated by use of Cauchy's theorem. Consider the integrand as a complex function of the complex variable η. This function is single valued in the complex η plane with a slit running between -1 and 1. The integrand is positive just below the slit and negative just above the slit. It is easy to see that

$$I = \frac{1}{4}\oint_C \sqrt{1 - \eta^2}\eta^2 \, d\eta \tag{B2}$$

where the contour C runs counterclockwise around the slit. This contour may be deformed into the large circle C' (Fig. B1) without changing the value of the integral.

Now expand the integrand in powers of $1/\eta$:

$$\sqrt{1 - \eta^2}\eta^2 = i\sqrt{1 - (1/\eta^2)}\eta^3 = i\eta^3 - (i\eta/2) - (i/8\eta) + \cdots \tag{B3}$$

The expansion converges for $|\eta| > 1$, therefore, converges on C'. The contour integral becomes equal to $2\pi i$ times the residue at the simple pole, therefore,

$$I = \tfrac{1}{4}2\pi i[-(i/8)] = \pi/16 \tag{B4}$$

The integral in the numerator of (24) is $(4/\pi)I = \frac{1}{4}$.

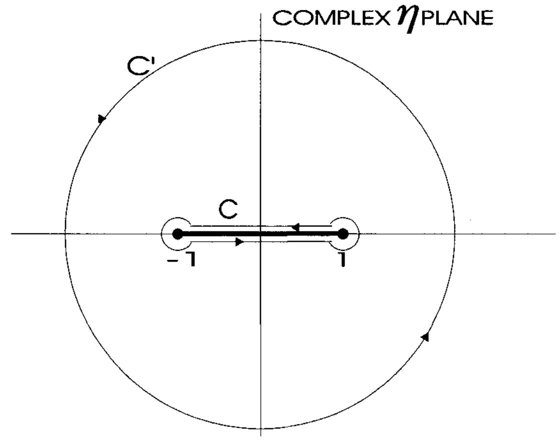

Fig. B1 Integration contours in the complex η plane.

References

[1]Seckel, E., *Stability and Control of Airplanes and Helicopters*, Academic, New York, 1964, p. 225.

[2]Katz, A., *Topics in Dynamics*, Lecture Notes, Univ. of Alabama Flight Dynamics Lab., 4th Printing, Pt. III, Tuscaloosa, AL, 1994.

[3]Evans, M., and Katz, A., "C++ Types for Three Dimensions," Univ. of Alabama Flight Dynamics Lab. (UA FDL), Rept. 93S01, Tuscaloosa, AL, 1993.

[4]Katz, A., and Evans, M., "C++ Types for Three Dimensions," *ACM Transactions on Software Engineering and Methodology* (submitted for publication).

Stable Cross-Type Parachute with Inflation Aid

Karl-Friedrich Doherr*

DLR, German Aerospace Research Establishment, D-38108 Braunschweig, Germany

Introduction

THE reduction of the minimum altitude needed for a safe release of personnel and payloads from low-flying aircraft is a real challenge to the parachute designer. The problem posed is to design a very reliable parachute system with short filling time, high drag coefficient, and little or no tendency to oscillate. In the following, a new parachute design is discussed that seems to have the potential to be used safely from low-flying aircraft and from helicopters as well.

Design of the LAP-LEONARDO Canopy

Several years ago Hoenen[1] invented a stable version of the cross parachute (German Patent DP 27 06 006 A1). The stabilizing effect was achieved by arms of trapezoidal shape plus horizontal slots between the roof and the four arms of the canopy (Figs. 1 and 2). This parachute (called STABKREUZ)

Presented as Paper 93-1201 at the RAeS/AIAA 12th Aerodynamic Decelerator Systems Technology Conference, London, England, UK, May 10–13, 1993; received June 26, 1994; revision received Dec. 28, 1994; accepted for publication Jan. 6, 1995.

*Head, Mathematical Methods and Data Handling Branch, Institute of Flight Mechanics. Member AIAA.